Synthesis, characterization, crystal structure, DNA- and HSA-binding studies of a dinuclear Schiff base Zn(II) complex derived from 2-hydroxynaphtaldehyde and 2-picolylamine

Zahra Kazemi, Hadi Amiri Rudbari, Valiollah Mirkhani, Mehdi Sahihi, Majid Moghadam, Sharam Tangestaninejad, Iraj Mohammadpoor-Baltork

Synthesis, characterization, crystal structure, DNA- and HSA-binding studies of a dinuclear Schiff base Zn(II) complex derived from 2-hydroxynaphtaldehyde and 2-picolylamine

Zahra Kazemi, Hadi
Amiri Rudbari, Valiollah Mirkhani, Mehdi Sahihi, Majid Moghadam, Sharam Tangestaninejad, I raj Mohammadpoor-Baltork

Department of Chemistry, University of Isfahan, Isfahan 81746-73441, Iran

Abstract

A tridentate Schiff base ligand NNO donor (**HL**: 1-((E)-((pyridin-2-yl)methylimino)methyl)naphthalen-2-ol was synthesized from condensation of 2-hydroxynaphtaldehyde and 2-picolylamine. Zinc complex, $\mathbf{Zn_2L_2(NO_3)_2}$, was prepared from reaction of $Zn(NO_3)_2$ and **HL** at ambient temperature. The ligand and complex were characterized by FT-IR, ^{1}H NMR, ^{13}C NMR and elemental analysis (CHN). Furthermore, the structure of dinuclear Zn(II) complex was determined by single crystal X-ray analysis. The complex, $\mathbf{Zn_2L_2(NO_3)_2}$, is centrosymmetric dimer in which deprotonated phenolates bridge the two Zn(II) atoms and link the two halves of the dimer. In the structure, Zinc(II) ions have a highly distorted six-coordinate structure bonded to two oxygen atoms from a bidentate nitrate group, the pyridine nitrogen, an amine nitrogen and phenolate oxygens. The interaction of dinuclear Zn(II) complex with fish sperm DNA (FS-DNA) and HSA was investigated under physiological conditions using fluorescence quenching, UV–Vis spectroscopy, molecular dynamics simulation and molecular docking methods. The estimated binding constants for the DNA-complex and HSA-complex were $(3.60 \pm 0.18) \times 10^4\ M^{-1}$ and $(1.35 \pm 0.24) \times 10^4\ M^{-1}$, respectively. The distance between dinuclear Zn(II) complex and HSA was obtained based on the Förster's theory of non-radiative energy transfer. Molecular docking studies revealed the binding of dinuclear Zn(II) complex to the major groove of FS-DNA and IIA site of protein by formation of hydrogen bond, π-cation and hydrophobic interactions.

Keywords

Dinuclear Zn(II) complex

Crystal structure

DNA interaction

HSA binding

Molecular modeling

Introduction

Nowadays, cancer is known as an important agent of worldwide death which can be cured by damage to DNA of cancer cells. An anti-cancer drug binds to DNA of cancer cells and inhibits DNA replication and transcription [1], [2]. Great investigations have been performed on metal-based pharmaceutical molecules since use of cisplatin as an anti-cancer drug [3]. The metal complexes have high affinity to DNA and can be introduced as anti-cancer drug candidates [4]. Moreover, literatures reported that the coordination of metal to ligand increases the biological activity of compounds [5], [6]. Schiff bases have attracted a great attention in bioinorganic field among other ligands due to their stability, biocompatibility and structural variability [4], [7].

Zinc(II) is the most abundant essential transition metal after Fe^{3+} in human body and many enzymes such as carboxypeptidase and carbonic anhydrase use Zinc(II) in their active sites [8], [9]. Hence it has attracted a great attention in medicine field [10] and many studies have been carried out on Zn(II) complex and its biological properties such as antimicrobial [11] and antitumor [12], [13], [14] activity. Some studies reported the bigger DNA binding constant for Zn in comparison to the other metals such as Cu and Ni [15]. Moreover, researches revealed that bimetallic complexes have higher affinity with DNA in contrast with their mononuclear complex analogue [16].

DNA is known as a major target for anticancer drugs. Thus, the study of interaction between Schiff base complexes and DNA is critical step to design and synthesis of new pharmaceutical molecules which is an active area of research [17], [18]. The small molecules including drugs can interact with DNA through three models: (I) electrostatic binding between cation species and negative charged DNA phosphate residues (II) interaction with grooves of DNA by hydrogen bond or van der Waals interactions, and (III) intercalative binding [19], [20], [21].

Human serum albumin (HSA) is the most abundant plasma carrier protein, which is involved in binding and transport drugs in the blood. Therefore, the first step to know the mechanism of anti-

cancer drug in body is the investigation its HSA binding. The Schiff base complexes as candidate for anti-cancer drugs have high affinity for binding to HSA [22], [23].

In this work, we have synthesized a new tridentate Schiff base ligand (**HL**) and its dinuclear Zinc(II) complex **$Zn_2L_2(NO_3)_2$** (see Scheme 1, Scheme 2). The schiff base ligand and its Zn(II) complex were characterized by FT-IR, ^{1}H NMR, ^{13}C NMR and elemental analysis. In addition, the molecular structure of complex was determined by single crystal X-ray diffraction technique. Furthermore, HSA and DNA binding of dinuclear Zn(II) complex was investigated using fluorescence quenching, UV–Vis spectroscopy, molecular dynamics simulation and molecular docking methods.

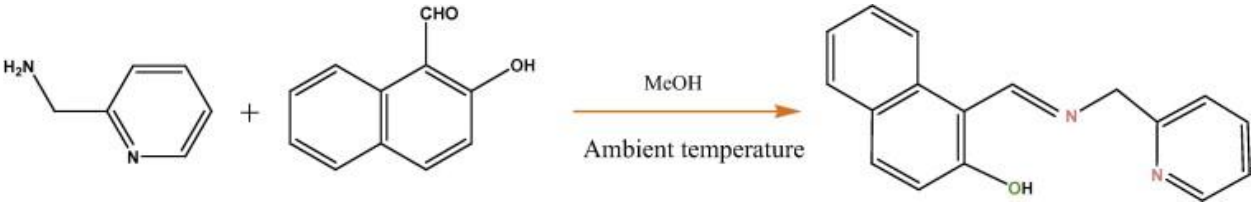

Scheme 1. Synthesis of Ligand (**HL**).

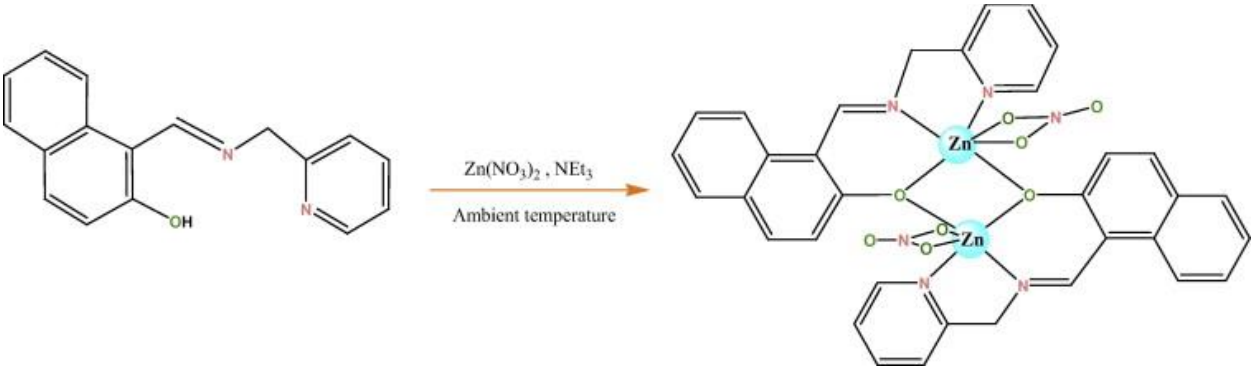

Scheme 2. Synthetic route for preparation of **$Zn_2L_2(NO_3)_2$** complex.

Experimental

Materials

Human serum albumin (HSA), fish sperm DNA, Tris(hydroxymethyl)-aminomethane (Tris) and ethidium bromide (3,8-diamino-5-ethyl-6-phenylphenanthridinium bromide, EtBr) were purchased from Sigma–Aldrich. 2-Hydroxy-1-naphtaldehhyde and 2-picolylamine were obtained from Merck chemical Co. and used without further purification. All salts used for buffer preparation were analytical grade and dissolved in double distilled water. All of the solutions were used freshly after preparation.

Apparatus and software

The FT-IR spectrum was recorded on a JASCO, FT/IR-6300 spectrometer (4000–400 cm^{-1}) in KBr pellets. ^{1}H and ^{13}C NMR spectra were recorded on a Bruker Avance 400 spectrometer using $CDCl_3$ as solvent for the ligand and DMSO for the Zn(II) complex. The UV–Vis spectra were recorded on a JASCO V-570 spectrophotometer. Fluorescence measurements were carried out on Shimadzu RF-5000 spectrofluorometer at room temperature.

Synthesis of Schiff base ligand

A methanolic solution (10 ml) of 2-Picolylamine (10 mmol) was slowly added to a solution of 2-hydroxy-1-naphtaldehyde (10 mmol) in absolute methanol (10 ml). Then the mixture was stirred at room temperature for 2 h. The reaction mixture was allowed to stand for slow evaporation of the solvent until the formation of yellow oil. After that the resulting yellow oil re-dissolved in a minimum amount of methanol and light yellow precipitate was extracted by diethyl ether. Yield 88%, Anal. Calc. for $C_{17}H_{14}N_2O$: C, 77.84; H, 5.38; N, 10.68. Found: C, 77.51; H, 5.71; N, 10.23.

FT-IR (KBr, cm^{-1}): (O H) 3365 (br, vs); (C N) 1620 (vs). ^{1}H NMR ($CDCl_3$, 400 MHz, 298 K) δ/ppm:13.13 (1H, s, O*H*),8.9 (s, 1H, N C*H*),8.5 (d, 1H, Ar), 8.2 (d, 1H, Ar), 7.9 (t, 1H, Ar), 7.7 (d, 1H, Ar), 7.6 (d, 1H, Ar), 7.5 (t, 1H, Ar), 7.4 (t, 1H, Ar), 7.2 (t, 1H, Ar), 7.0 (d, 1H, Ar), 6.9 (10H, Ar), 4.8 (s, 2H, CH*H*). ^{13}C NMR ($CDCl_3$, 400 MHz, 298 K) δ/ppm: 175.1, 164.8, 158.0, 149.4, 139.1, 137.1, 129.4, 129.1, 128.0, 124.4, 124.0, 122.9, 121.9, 119.0, 118.4, 118.1, 58.3.

Synthesis of Zn(II) complex

Methanolic solution (10 ml) of 2-hydroxy-1-naphtaldehyde (5 mmol) was added dropwise to a methanolic solution (10 ml) of 2-picolylamin (5 mmol). The mixture was stirred for 2 h at room temperature. Then a solution of triethylamine (7 mmol) in absolute methanol (5 ml) was added to the mixture. The mixture stirred for 10 min, and then a solution of $Zn(NO_3)_2 \cdot 6H_2O$ (10 mmol) in absolute MeOH (10 ml) was added dropwise. Upon addition, immediate precipitation of **$Zn_2L_2(NO_3)_2$** complex occurs. The resulting solution was stirred for 2 h in ambient temperature. The yellow powder was isolated from the solution and purified by washing with cold methanol. Appropriate single crystals for X-ray crystallography were obtained in methanol by recrystallization. The yield was 86%, Anal. Cal. for $Zn_2C_{34}H_{26}N_6O_8$: C, 52.53, H 3.37, N10.81.

Found: C, 52.58, H, 3.52, N, 10.72. FT-IR (KBr, cm^{-1}): (C N) 1623 (vs). ^{1}H NMR (DMSO,

400 MHz, 298 K) δ/ppm: 9.5 (s, 1H, N C*H*); 8.5 (d, 1H, Ar), 8.2 (d, 1H, Ar),8.1 (t, 1H, Ar),8.0 (d, 1H, Ar), 7.9 (d, 1H, Ar), 7.8 (d, 1H, Ar), 7.6 (t, 1H, Ar), 7.4 (t, 1H, Ar), 7.2 (t, 1H, Ar), 6.9 (d, 1H, Ar), 5.3 (s, 2H, CH_2). ^{13}C NMR ($CDCl_3$, 400 MHz, 298 K) δ/ppm: 171.6, 164.9, 156.2, 147.3, 139.9, 135.2, 135.0, 128.7, 127.3, 126.7, 125.4, 123.6, 123.1, 121.3, 118.9, 108.0and 56.7.

Single crystal diffraction method

The X-ray diffraction measurement for Zn(II) complex, **$Zn_2L_2(NO_3)_2$**, was made on a STOE IPDS-II diffractometer with graphite monochromated Mo Kα radiation. A yellow small crystal was mounted on a glass fiber and used for data collection. Data were collected at a temperature of 298 K and in a series of ω scans in 1° oscillations and integrated using the Stoe X-AREA software package [24]. A numerical absorption correction was applied using X-RED [25] and X-SHAPE [26] softwares. The data was corrected for Lorentz and Polarizing effects. Structure was solved by direct methods using SIR2004 [27]. The non-hydrogen atoms were refined anisotropically by the full matrix least squares method on F^2 using SHELXL [28]. All the hydrogen (H) atoms were placed at the calculated positions and constrained to ride on their parent atoms. Crystallographic data are listed in Table 1. Selected bond distances and angles are summarized in Table S1.

Table 1. Crystal data and structure refinement for **$Zn_2L_2(NO_3)_2$**.

Empirical formula	$C_{34}H_{26}N_6O_8Zn_2$
Formula weight	777.35
Temperature	298(2) K
Wavelength	0.71073 Å
Crystal system	Orthorhombic
Space group	Pbca
Unit cell dimensions	a = 14.517(3) Å
	b = 14.626(3) Å
	c = 15.449(3) Å
Volume	3280.1(11) Å^3
Z	4
Density (calculated)	1.574 Mg/m^3
Absorption coefficient	1.525 mm^{-1}
F(0 0 0)	1584
Theta range for data collection	2.38–25.00°
Index ranges	$-17 \leqslant h \leqslant 17$
	$-17 \leqslant k \leqslant 17$

	$0 \leqslant l \leqslant 18$
Reflections collected	10,844
Independent reflections	2895 [$R_{(int)} = 0.0327$]
Data completeness	100.0%
Refinement method	Full-matrix least-squares on F^2
Data/restraints/parameters	2895/0/226
Goodness-of-fit on F^2	0.805
Final R indices [$I > 2\sigma(I)$]	$R_1 = 0.0280$
	$wR_2 = 0.0471$
R indices (all data)	$R_1 = 0.0675$
	$wR_2 = 0.0520$
Largest diff. peak and hole	0.136 and −0.255 e Å^{-3}

DNA binding studies

The stock solution of FS-DNA was prepared in 50 mM Tris buffer at pH 7.5 using double-distilled deionized water and stored at 4 °C. The FS-DNA concentration was determined by the absorption intensity at 260 nm and the molar absorption coefficient 6600 M^{-1} cm^{-1}. Purity of FS-DNA solution was confirmed by ratio of UV absorbance at 260 and 280 nm ($A_{260}/A_{280} = 1.9$), indicating that FS-DNA is free from protein impurity [29], [30]. A stock solution of the Zn(II) complex was prepared by dissolving the complex in an aqueous solution of DMF as the co-solvent and then diluted suitably with the corresponding buffer to the required concentrations. The final DMF concentration never exceeded 0.3% v/v. The UV–Vis spectral features of dinuclear Zn(II) complex

did not change on keeping its buffered or DMF solution for 24 h and no precipitation or turbidity was observed even after long storage at room temperature (at least 4 weeks after preparation), which indicates the stability of the Zn(II) complex in different media. UV–Vis absorption spectra of Zn(II) complex (2×10^{-5} M) in absence and presence of various amounts of DNA (0–67 μM) were recorded. All complex–DNA solutions were allowed to incubate for 5 min before recording the absorption spectra and then the absorptions were recorded to calculate the intrinsic binding constant, K_b of the dinuclear Zn(II) complex to FS-DNA.

Furthermore, fluorescence quenching experiments carried out using quartz cuvette with 1 cm optical path length and the excitation and emission slits set at 5 and 10 nm, respectively. To this aim, the FS-DNA solution was stirred with EtBr with molar ratio of DNA:EtBr 10:1 for 1 h at 4 °C. Then, various amounts of Zn(II) complex (0–45 μM) were added to this mixture. The fluorescence spectra were measured in the range of 550–650 nm with exciting wavelength at 520 nm. In each measurement after addition of FS-DNA, the mixture was allowed to stand for 5 min.

HSA Binding experiments

A stock solution of HSA was prepared by dissolving the desired amount of HSA in 50 mM phosphate buffer (pH = 7). The HSA stock solution was stored at 4 °C in the dark and used within 2 h. HSA concentration was determined by UV–Vis spectrophotometry using the molar absorption coefficient 35700 M^{-1} cm^{-1} at 278 nm [31]. UV–Vis spectra of dinuclear Zn(II) complex were recorded with addition of successive amount of HSA with molar ratios of the [HSA]/[Complex] = 0–4.5 at room temperature. Fluorescence quenching experiment was also done to more investigation of interaction between HSA and Zn(II) complex. In this experiment 2 mL of HSA solution (4 μM) was placed into the cell and various amounts of 100 μM dinuclear Zn(II) complex were added to the cell. The fluorescence intensity was measured with excitation wavelength at 295 nm and emission wavelength rang of 300–370 nm. As mentioned above, the mixture was allowed to incubate for 5 min after addition of HSA or complex.

Molecular dynamics simulation

The known crystal structures of DNA (PDB ID: 423D) with sequence $d(ACCGACGTCGGT)_2$ and HSA (PDB ID: 1BM0) were taken from the Brookhaven Protein Data Bank (www.rcsb.org). A

10 ns MD study was carried out using GROMACS4.5.6 package [32], [33] and GROMOS96 43a1 force field [34], [35] for DNA and HSA. The topology parameters of DNA and HSA were generated using gromacs. The macromolecules were located in a cubic box with the periodic boundary conditions. The SPC water model [36] was employed for the water molecules. The sufficient amounts of sodium ions were added to balance the charge of system. The system was energy-minimized using the steepest descent method for the 4000 time-step [37]. Next, position restraint procedure was performed in NVT and NPT ensembles with time duration of 200 ps. The system was equilibrated at constant temperature of 300 K and constant pressure of 1.0 bar. Finally, a 10 ns MD simulation was carried out at 1 bar and 300 K. The Particle-Mesh Ewald (PME) method [38], [39] and the cut-off method were used for the long-range electrostatic interactions and the van der Waals interactions, respectively. A 7 Å cutoff for the van der Waals interactions was used. The equation of motion was integrated by the leap-frog algorithm with the 2 fs time-step and the atomic coordinates were recorded to the trajectory file every 0.5 ps for further analysis. The stability of simulated systems was scanned using the root-mean-square deviations (RMSDs) of HSA and DNA with respect to their initial structures. The average RMSD values of the HSA and DNA backbones were 8.21 nm and 5.39 nm, respectively. The equilibrated conformation of the HSA and DNA were used for docking.

Docking procedure

Docking study was carried out to indicate the active binding site for dinuclear Schiff base Zn(II) complex. The 3D structure of the metal complex was generated using the CIF file of its X-ray crystal structure. The CIF file was converted to the PDB format by using the Mercury software. The equilibrated conformations of the HSA and DNA in MD simulation were used for docking and missing hydrogen atoms were added at appropriate geometry. Flexible-ligand docking was performed by AutoDock 4.2 molecular-docking program using the implemented empirical free energy function and the Lamarckian Genetic Algorithm [40]. The Gasteiger charges were added to prepare the macromolecule input file for docking and the Auto Grid was used to calculate Grids. A grid map with $90 \times 90 \times 90$ points and a grid-point spacing of 0.375 Å was applied in all dockings. 200 docking runs with 25,000,000 energy evaluations for each run were performed.

Result and discussion

IR spectra

The comparison of IR spectrum of ligand with complex is an evidence for the coordination of metal to ligand. The sharp band assigned to imine group is observed at 1620 cm^{-1} for free ligand and at 1623 cm^{-1} for binuclear complex.

The absorption band at 1367 cm^{-1} and 1472 cm^{-1} in the spectrum of free ligand can be assigned to

C O and C N stretching of the ligand respectively. However, after coordination of the metal ion to the ligand via oxygen and nitrogen, these bands shifted to 1336 cm^{-1} and 1455 cm^{-1}.

Furthermore, elimination of the stretching frequency of O H group after complexation is result of deprotonation of the ligand [41].

NMR study

^{1}H NMR and ^{13}C NMR spectra of schiff base ligand and $\mathbf{Zn_2L_2(NO_3)_2}$ complex were measured in $CDCl_3$ and DMSO, respectively. The structure of $\mathbf{Zn_2L_2(NO_3)_2}$ is symmetric, therefore ^{1}H NMR and ^{13}C NMR of two coordinated ligands is identical.

The singlet peak due to the imine proton in the ligand was observed at 8.9 ppm which shifted to 9.5 ppm for $\mathbf{Zn_2L_2(NO_3)_2}$ complex. The resonance signal observed at 13.13 ppm assign to OH group that is not observed in the ^{1}H NMR spectrum of complex. It confirms that the hydroxyl groups are fully deprotonated and the oxygen acts as a coordination atom. In ^{13}C NMR of schiff base ligand, the peak at 175.1 ppm assignable to the imine carbon atoms, confirms the presence of the Schiff base ligand in the complexes [41]. The ^{1}H NMR spectrum of complex shows a peak at 5.3 ppm assigned to H_5 (Fig. S1). Also, aromatic protons of Zn(II) complex appear in the region of 6.9–8.5 ppm (see Fig. 1).

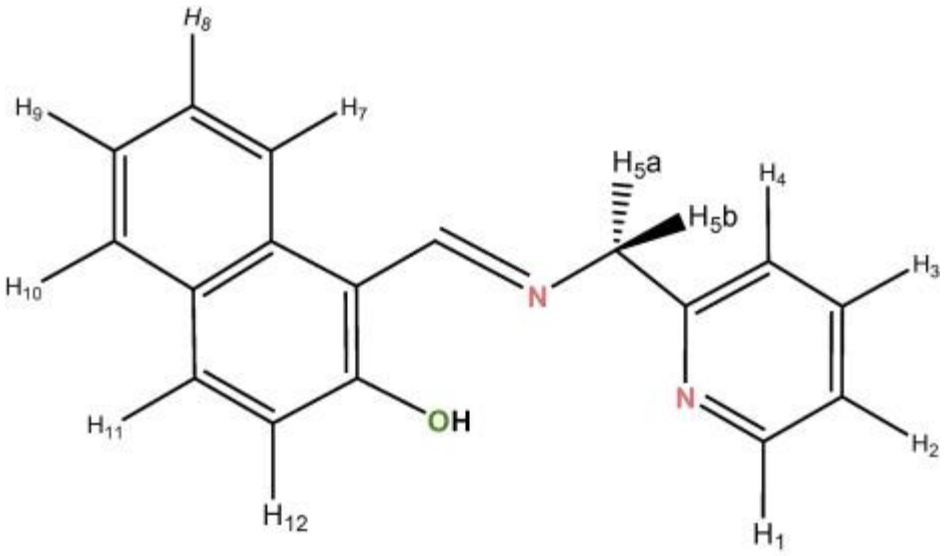

Fig. 1. Molecular structure of **HL** showing the lettering scheme for NMR assignments.

X-ray structure

The crystal structure of $\mathbf{Zn_2L_2(NO_3)_2}$ consists of a discrete centro-symmetric dimeric unit (Fig. 2). Selected bond length sand angles are summarized in Table S1 in supplementary. The dinuclear unit is formed by two Zn(II) atoms labeled Zn(1) and Zn(1′) (′ = −*x*, −*y* + 1, −*z*), bridged by the two phenoxo oxygen atoms O(1) and O(1′) of the Schiff-base ligands, **L**. Each of the two equivalent zinc atoms presents a distorted octahedral environment formed by the deprotonated chelate Schiff base ligand, a bidentate nitrate anion and a phenoxo oxygen atom from the symmetry related Schiff base ligand (Fig. 2). The Schiff base ligand coordinates the Zn(II) ion in facial (*fac*) configuration through the imine nitrogen N(1), the nitrogen atom of pyridine N(2), and the phenoxo oxygen atom O(1) with usual phenoxo-bridged bond distances (Table S1 in supplementary) [42]. Note that the double oxo bridge connecting both Zn(II) ions is slightly asymmetric because each Zn(II) ion is closer to its own phenoxo oxygen atom (Zn(1) O(1) = 2.0188(18) Å) than to the phenoxo oxygen atom of the symmetry related Schiff base (Zn(1) O(1′) = 2.0611(16) Å). The two Zn atoms are separated by 3.1428(7) Å and the Zn O(1) Zn′ angle is 100.76(7)°.

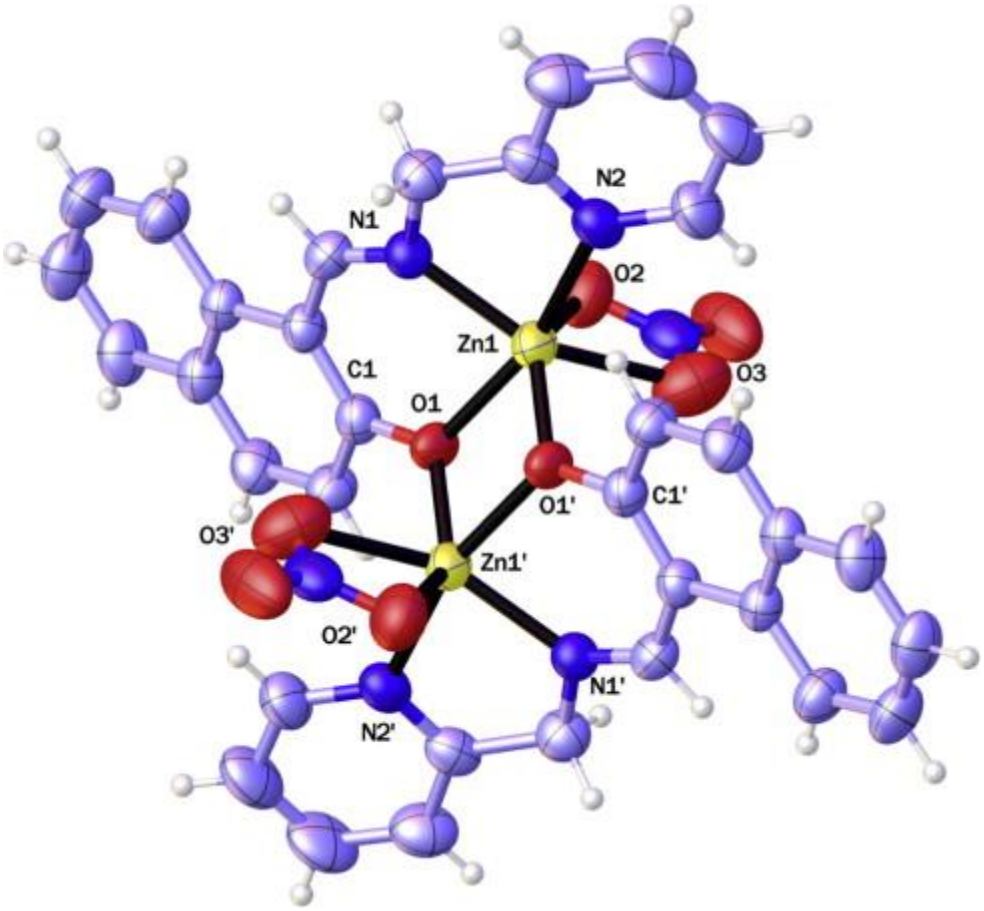

Fig. 2. ORTEP representation of **$Zn_2L_2(NO_3)_2$**. Displacement ellipsoids are drawn at the 50% probability level and H atoms are shown as small spheres of arbitrary radii.

The nitrate group acts as an asymmetric bidentate ligand with Zn(l) O(2) = 2.206(2) and Zn(l)

O(3) = 2.343(3) Å. These distances are similar to that reported by Tandon et al. for Zn(II) complex involving bidentate nitrate [42].

As we know, non-covalent interactions are at the core of most chemical and biological processes and hence knowledge of their nature, strength, occurrence and consequences is of paramount

importance [43]. The weak non-covalent interactions such as C H···X (X = O, N, S, halogen) and π–π stacking, while weaker than the classical H-bonds, also play notable roles in conformation, crystal packing, supramolecular assembly and physicochemical properties and thus have implications in drug design, material design and supramolecular synthesis [43], [44], [45], [46], [47], [48], [49].

Although there are not classical hydrogen bonds in the structure, but both uncoordinated oxygen atoms of the nitrate ions are involved in C H···O non-classical hydrogen bonds (Fig. 3). Non-classical intermolecular hydrogen bond occurs between C(6) H(6)···O(4) [2.58 Å] atoms and C(16) H(16)···O(2) [2.49 Å] atoms (Fig. 3).

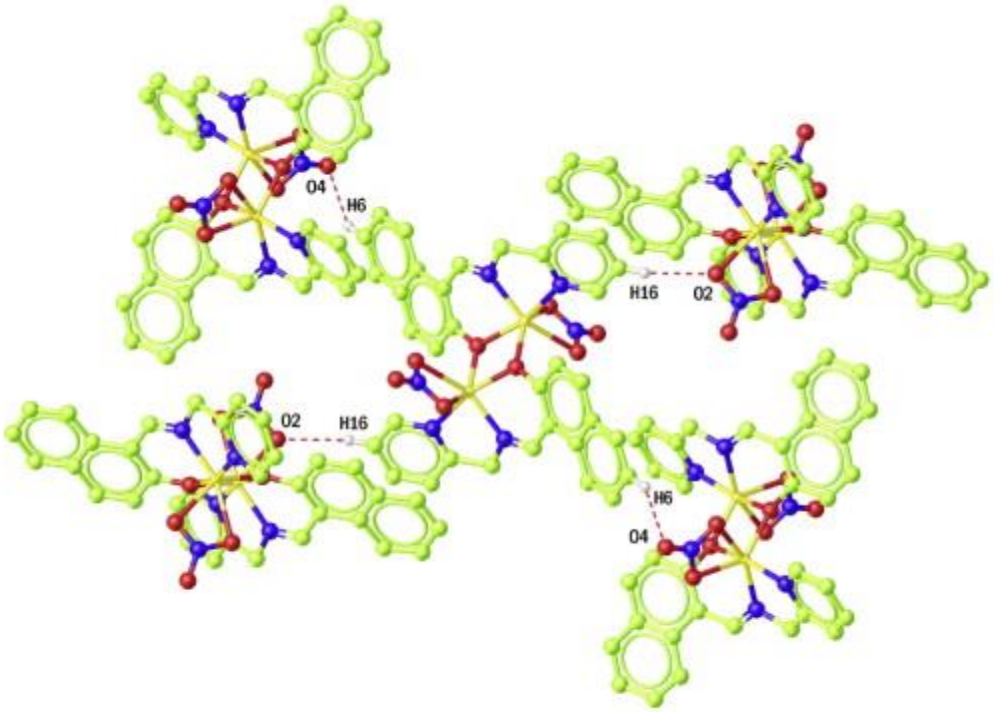

D—H...A	D—H	H...A	D...A
C(6)—H(6)...O(4)	0.93	2.58	3.407(4)
C(16)—H(16)...O(2)	0.93	2.49	3.388(4)

Fig. 3. Intramolecular hydrogen bond geometries (Å, °).

Another interesting feature of the **$Zn_2L_2(NO_3)_2$** complex is the presence of C H···π and π···π interactions (Fig. 4, Fig. 5). Weak C H···π edge-to-face interactions are present between CH of Schiff base group with H···π distance of 2.67 Å for C(12) H(12B)···Cg(9) [Cg(9) is centroid for C(4)/C(9) ring] (Fig. 4). Also, in the crystal packing π···π interactions are exist between the

naphthalene ring and pyridine ring of neighbor molecule, Cg(7)···Cg(9), with centroid–centroid distance of 3.5498(14), 3.5082(12) Å, in which Cg(7) and Cg(9) are centers of N(2) C(13) C(14) C(15) C(16) C(17) and C(4) C(5) C(6) C(7) C(8) C(9) rings, respectively (Fig. 5, Scheme 3).

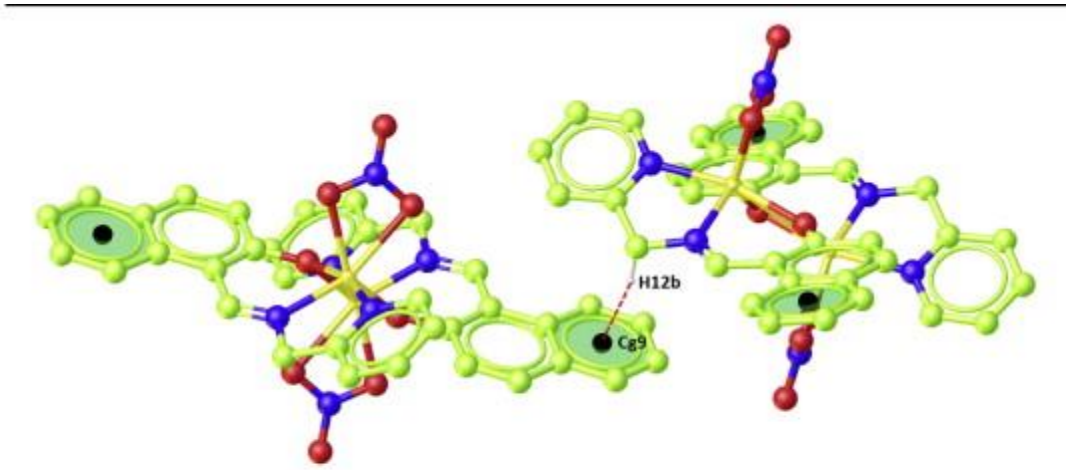

X—H(I)…Cg(J)*	H…Cg	X…Cg	X—H…Cg	Symmetry code
C(12)—H(12B) …Cg(9)	2.67	3.580(3)	156	1-X,-1/2+Y,1/2-Z

* Cg(9): C(4)/C(9) ring.

Fig. 4. Analysis of X H···Cg (Pi-Ring) Interactions (H···Cg < 4.0 Å).

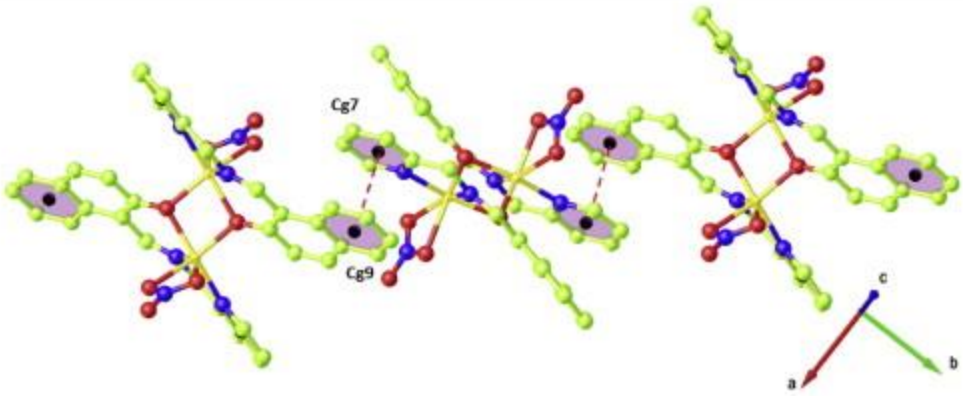

Cg(I)–Cg(J)	d_{Cg-Cg}[a]	α[b]	β, γ[c]	$d_{plane-plane}$[d]	d_{offset}[e]	Symmetry codes
Cg(7)…Cg(9)	3.5838(19)	5.45(15)	11.79, 7.90	3.5498(14), 3.5082(12)	0.732, 0.492	1/2-X,-1/2+Y,Z

[a] Centroid–centroid distance. [b] Dihedral angle between the ring plane. [c] Offset angles: angle between Cg(I)–Cg(J) vector and normal to plane I, angle between Cg(I)–Cg(J) vector and normal to plane J (β = γ when α = 0). [d] Perpendicular distance of Cg(I) on ring J and perpendicular distance of Cg(J) on ring I. [e] Horizontal displacement between Cg(I) and Cg(J), two values if the two rings are not exactly parallel (α ≠ 0). Cg(7): centroid of N(2)–C(13)–C(14)–C(15)–C(16)–C(17); Cg(9): centroid of C(4)–C(5)–C(6)–C(7)–C(8)–C(9).

Fig. 5. Aromatic interaction parameters (Å and °) for description of π–π interactions.

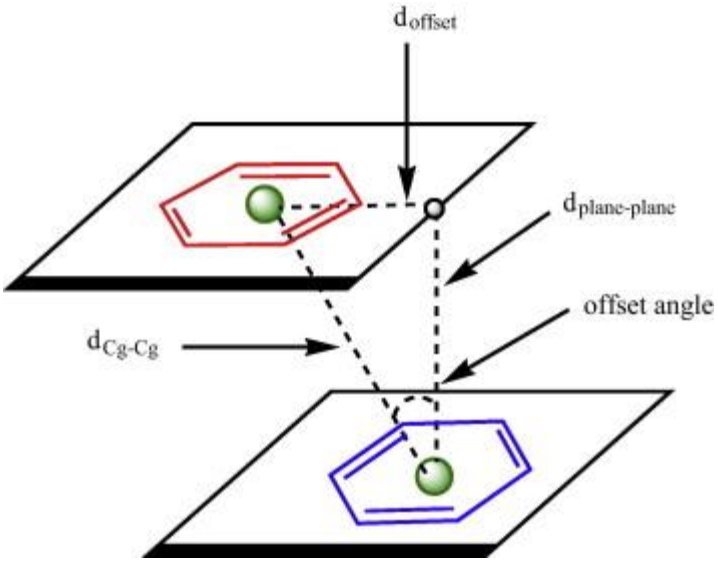

Scheme 3. Schematic representation of geometrical parameters for definition of π···π stacking between two rings in **$Zn_2L_2(NO_3)_2$.**

DNA binding studies

DNA interactions play an important role in the field of medicinal chemistry, since it is the primary intracellular target of anticancer drugs. The interaction between small molecules and DNA can cause DNA damage in cancer cells, blocking the division of cancer cells, and resulting in cell death. It includes conformational and structural changes of DNA molecules which play an important role in the biological systems. Thus, to further demonstrate the mechanism of anticancer action of the dinuclear Zn(II) complex, its interaction with FS-DNA was analyzed by spectroscopic techniques.

UV–Vis absorption

Recording UV–Visible spectrum of metal complex upon addition of various amount of DNA is a powerful technique to investigate DNA binding of complex. Electronic absorption spectra can give the information regarding the electronic perturbations in the complex made by interaction with DNA [50]. Generally, hyperchromic or hypochromic effect and red or blue shift are observed in the UV–Vis spectra of drugs upon binding of drugs to DNA. Hypochromic and red shift are indicative of intercalation mode [51]. Intercalation mode is interaction between π^*-orbital of complex with π-orbital of DNA base pairs. Therefore, energy level of π^*-orbital of complex decreases which causes red shift in UV–Vis spectrum of complex. Furthermore, the coupled π^*-orbital is filled and so the probability of electron transition decreased and hypochromic is observed [51], [52]. On the other hand, hyperchromic effect in spectrum of drug is due to damage of the DNA double-helix structure [53]. This change in spectrum can be attributed to groove binding or electrostatic interaction. The minor or major groove binding causes damage to DNA at the exterior phosphate backbone [53], [54].

The absorption spectrum of the synthesized Zn(II) complex indicates two absorption bands attributed to $\pi \rightarrow \pi^*$ and $n \rightarrow \pi^*$ at 305 and 380 nm. The $n \rightarrow \pi^*$ absorption band was chosen to determine the interaction of this complex with DNA. Through addition of various amount of FS-DNA (1.5×10^{-4} M) with molar ratio of [DNA]/[Complex], 0–6, a hypochromic effect accompanied by red shift in spectrum of complex is observed (Fig. 6).

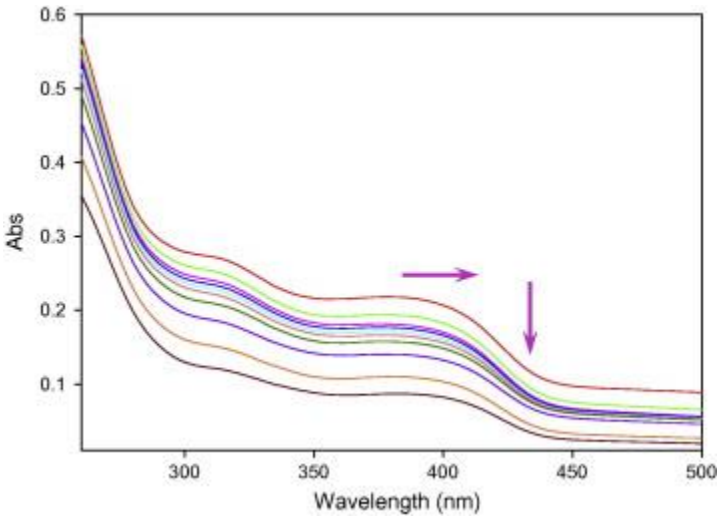

Fig. 6. Electronic absorption spectra of Zn(II) complex upon addition of various amounts of DNA. [Complex] = 2×10^{-5} M, [DNA] = 1.5×10^{-4} M.

Although, observation a hypochromic effect in UV–Vis spectrum with increase amount of DNA reveals an intercalative mode, some studies reported that this is not a correct conclusion necessarily. The hypochromic effect can be observed as a result of other binding mode such as groove binding due to the changes in the solvent distribution and the orientation effect in moving into the more hydrophobic environment of groove [55], [56]. The crystal structure of the complex (Fig. 2) shows that this complex is not planner. Hence, probability of intercalation for this complex is very low. This spectral characteristic suggests that this complex interacts with FS-DNA through the partial insertion of the ligand aromatic rings to the FS-DNA groove. Moreover, the small red-shift may be attributed to the groove binding affinity of the complex which is due to the presence of a phenyl ring in the coordinated ligand [57].

To assess the binding ability of the dinuclear Zn(II) complex with FS-DNA, the intrinsic binding constant (K_b) was determined using following equation [21]:

$$\frac{[\mathrm{DNA}]}{\varepsilon_a - \varepsilon_f} = \frac{[\mathrm{DNA}]}{\varepsilon_b - \varepsilon_f} + \frac{1}{K_b(\varepsilon_b - \varepsilon_f)} \quad (1)$$

where [DNA] is the concentration of FS-DNA; ��, ��, and ��, are the apparent extinction coefficient, the extinction coefficient for free metal and the extinction coefficient for the complex

in fully bound form, respectively. ⬚⬚ was determined by calibration curve and ⬚⬚ is the ratio of A_{obs} to [Complex]. A plot of [DNA] vs [DNA]⬚⬚-⬚⬚ gives K_b as ratio of slop to y-intercept. The binding constant of FS-DNA and dinuclear Zn(II) complex is $3.3 \times 10^4\ M^{-1}$ which is comparable to obtained data for the other dinuclear Zn(II) complexes. Patel et al. reported the K_b value for synthesized homo dinuclear Zinc complexes and DNA in the range of $(1–3.5) \times 10^4\ M^{-1}$ [58].

The obtained data are lower than the mentioned K_b for classical intercalators (ethidium bromide and [Ru(phen)DPPZ]) that their binding constants are in the order of $10^6–10^7\ M^{-1}$ [59]. Therefore, the synthesized Schiff base complex can be bind to FS-DNA via groove binding.

Fluorescence quenching experiment

EtBr emits only a weak fluorescence emission in solution due to hydrogen transfer from one of amino group of EtBr into solution which causes nonradiative decay, while a significant increase of fluorescence intensity of EtBr is observed with the addition of FS-DNA. Since the EtBr molecules can be intercalated into the double helix of DNA [60], [61], [62], [63]. In the present study, quenching fluorescence of DNA-EtBr by addition of Zn(II) Schiff base complex is measured (Fig. 7). The absorptions of the dinuclear Zn(II) complex at the excitation and emission wavelengths were approximately zero in all concentrations. Hence, a reduction in the emission intensity is independent of the inner filter effect. However, this complex cannot intercalate to the DNA duplex, but it can displace EtBr in a non-competitive manner by changing the DNA conformation. Consequently, the DNA-bound EtBr molecules are converted to their free form in solution. In order to determine the binding ability between the complex and FS-DNA, the Stern–Volmer quenching plot was obtained by monitoring the fluorescence quenching of the EtBr-DNA with increasing the concentration of the Zn(II) complex according to the Stern–Volmer equation [64]:

$$\frac{F_0}{F} = 1 + K_{sv}[Q] = 1 + K_q\tau[Q] \qquad (2)$$

where F_0 and F are the fluorescence intensity of FS-DNA in absence and presence of Zn(II) complex, and K_{sv} is the Stern–Volmer quenching constant, K_q is the quenching rate constant of DNA and τ is the average lifetime of DNA without quencher which is typically equal to 10^{-8} s for biomacromolecules [65]. K_{sv} is determined from the plot of F_0/F vs [Q]. In the present

study, K_{sv} was obtained 1.9×10^4 M^{-1} (Fig. 8). The value of K_{sv} shows that this complex has high quenching efficiency and a significant degree of binding to FS-DNA. Fluorescence quenching is classified to two mechanisms: static quenching and dynamic quenching. In the static mechanism, the fluorophore and the quencher collide together in the ground state while fluorophore and quencher collide together in the excited state in dynamic mechanism [65]. Linearity of the Stern–Volmer plot indicates that quenching fluorescence has only one mechanism, dynamic or static [66]. In this study, the value of K_q was obtained 1.9×10^{12} M^{-1} S^{-1} that is greater than limiting diffusion rate constant of the diffusional quenching for biopolymers (2×10^{10} M^{-1} S^{-1}). This observation supports that quenching fluorescence of DNA occurs by static mechanism [65].

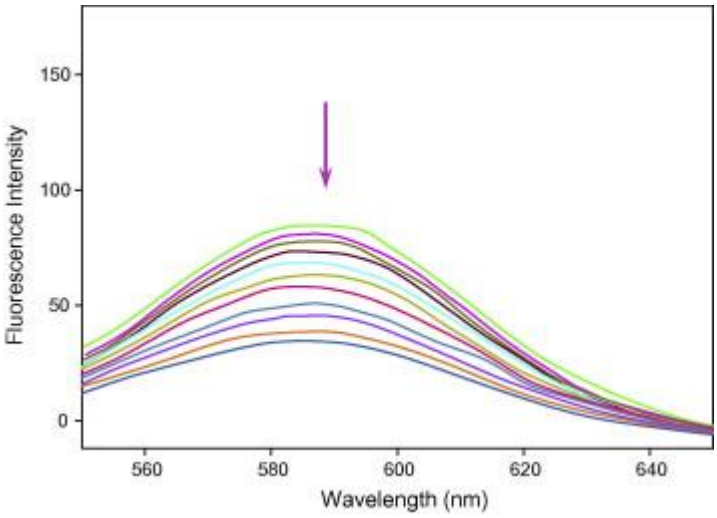

Fig. 7. Emission spectra of the EtBr-DNA system in the absence and presence of the various concentrations of Zn(II) complex. [DNA] = 10^{-4} M, [EtBr] = 10^{-5} M,

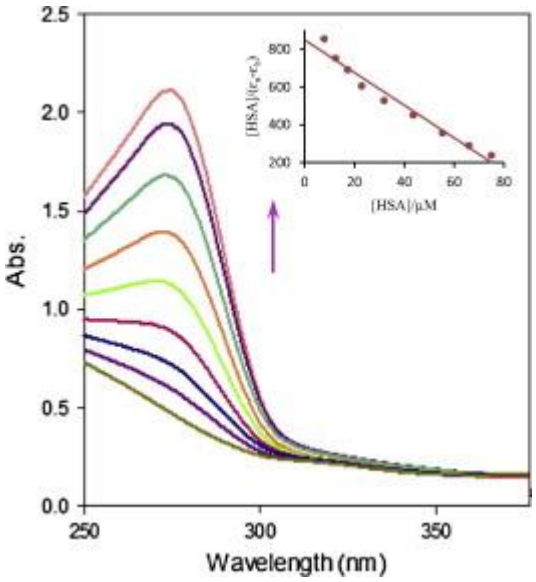

Fig. 8. Electronic absorption spectra of Zn(II) complex upon addition of various amount of HSA. [Complex] = 2×10^{-5} M, [HSA] = 1.5×10^{-4} M.

Moreover, binding constant (K_b) of the Zn(II) complex and FS-DNA can be calculated by this experiment using following equation [65]:

$$\mathrm{Ln}\left(\frac{F_0-F}{F}\right) = \mathrm{Ln}K_b + n\mathrm{Ln}[Q] \quad (3)$$

where F_0 and F are the fluorescence intensity of FS-DNA in absence and presence of Schiff base complex, respectively. [Q] is the concentration of quencher that quencher is Zn(II) Schiff base complex here. "K_b" is obtained from the plot of Ln [Q] vs Ln$\blacklozenge$0-$\blacklozenge\blacklozenge$ as a slope. Furthermore, "n" which is the number of binding site per nucleic acid is y-intercept of the plot. The intrinsic binding constant (K_b) of Zn(II) Schiff base complex and FS-DNA is 3.9×10^4 M^{-1} and (n) is 0.72 (Fig. S2). This result is in good agreement with the UV–Vis spectroscopy result. Also, Eq. (4) can be used to investigate the apparent binding constant (K_{app}).

$$K_{app} \times [\mathrm{complex}]_{50} = K_{\mathrm{EtBr}} \times [\mathrm{EtBr}] \quad (4)$$

where $[\mathrm{complex}]_{50}$ is the concentration of complex that makes a 50% reduction of the initial fluorescence intensity of the EtBr-DNA system, $\blacklozenge$EthBr = 1×10^7 M^{-1} is the binding constant of EtBr with DNA and [EtBr] = 1×10^{-5} M [67]. The apparent binding constant was obtained as

$2.2 \times 10^6\ M^{-1}$ which is lower than the binding constant of classical intercalators and metallointercalators [68].

HSA binding studies

The drug–HSA interactions in the blood stream can influence the chemical stability, toxicity, and distribution of the drug. These interactions significantly influence the pharmacokinetics and pharmacodynamics of drugs. Consequently, it is important to know the binding affinity of HSA for drugs. Hence, the interaction of the dinuclear Zn(II) complex with HSA was investigated using fluorescence quenching and UV–Vis absorption spectroscopy.

Electronic absorption spectroscopy

UV–Vis absorption spectroscopy is an effective technique to study of HSA-drug binding. The titration of complex with increasing amount of HSA with the molar ratio of [HAS]/[Complex] = 0–4.5 was carried out and its absorption spectra were measured (Fig. 8). Eq. (1) was applied to obtain constant binding of HSA and dinuclear Zn(II) complex. All of calculations and definitions are similar to DNA binding study. Constant binding was calculated as $1 \times 10^4\ M^{-1}$.

Fluorescence spectroscopy

Fluorescence of HSA protein is originated from three amino acids, i.e. tryptophan (Trp), tyrosine (Tyr), and phenylalanine (Phe) residues. Fluorescence is a useful approach for investigating intermolecular interactions because of the photophysical character of the fluorophoreis sensitive to the polarity of its surrounding environment [69].

Decrease of fluorescence intensity through the addition of complex can confirm the binding of dinuclear Zn(II) complex to HSA [70]. Fig. 9 represents the fluorescence quenching of 3.5 μM HSA at the presence of various amount of dinuclear Zn(II) complex with molar ratio of [Complex]/[HSA] = 0–13. The fluorescence intensities were used in order to study the quenching mechanism between the Zn(II) complex and HSA. The fluorescence quenching data were analyzed using the Stern–Volmer equation. The inset of Fig. 9 represents the Stern–Volmer plot for binding of dinuclear Zn(II) complex to HSA. As a result, K_{sv} is calculated $3.8 \times 10^4\ M^{-1}$. Moreover, $K_q = 3.8 \times 10^{12}\ M^{-1}\ S^{-1}$ that is larger than maximum collision quenching constant ($2 \times 10^{10}\ M^{-1}S^{-1}$) of various quenchers with the biomacromolecules. This result represents the

existence of static quenching mechanism. Comparing obtained results from fluorescence quenching with UV–Vis absorption showed an agreement between them and represent high affinity of HSA for dinuclear Zn(II) complex binding.

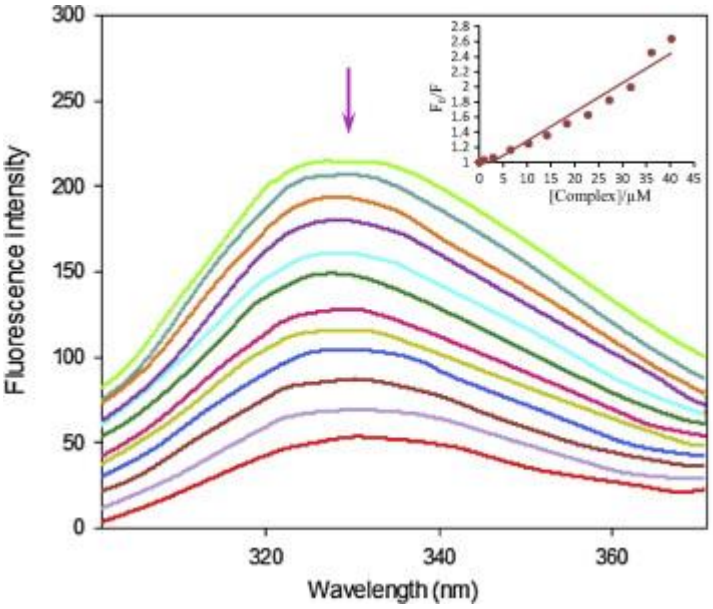

Fig. 9. Changes in the fluorescence spectra of HSA in the presence of Zn(II) complex. [HSA] = 4×10^{-6} M, λ_{ex} = 295 nm.

The binding constant (K_b) of the metal complex and HSA can be calculated using Eq. (3). The K_b value is calculated as 1.7×10^4 M^{-1} and n is determined as 1.1 (Fig. S3).

Energy transfer between dinuclear Zn(II) complex and HSA

Fluorescence resonance energy transfer (FRET) also known as Förster's resonance energy transfer is an interaction between the excited molecule and its adjacent molecule. Upon this interaction, non-radiative energy transfer take places from a donor molecule in excited state to an acceptor in ground state [71], [72]. According to this theory, Three conditions are required to energy transfer: (1) the donor should have fluorescence, (2) the fluorescence emission spectrum of the donor and the UV–Vis spectrum of the acceptor should have sufficient overlap and (3) the small distance between donor and acceptor (<8 nm) [72]. The distance and efficiency of energy transfer (E) between tryptophan residue of protein (HSA) and drug (complex) has been calculated using this theory through the following equation:

$$E = 1 - \frac{F}{F_0} = \frac{R_0^6}{R_0^6 + r^6} \quad (5)$$

where F_0 and F are fluorescence intensities of HSA in the absence and presence of complex, respectively and R_0 is the critical distance when the transfer efficiency is 50%; r is the distance between donor and acceptor. R_0 can be calculated by Eq. (6) [73]:

$$R_0^6 = 8.79 \times 10^{-25} K^2 N^{-4} J\varphi \quad (6)$$

In the above equation, the term K^2 is the orientation factor of the dipoles; is the refracted index of medium, J is the overlap integral of the fluorescence spectrum of the donor with absorption spectrum of the acceptor and φ is the fluorescence quantum yield of the donor. The value of J can be calculated by the following expression:

$$J = \frac{\sum F(\lambda)\varepsilon(\lambda)\lambda^4 \Delta\lambda}{\sum F(\lambda)\Delta\lambda} \quad (7)$$

where $F(\lambda)$ is the fluorescence intensity of the donor in the absence of the acceptor at wavelength λ and ε is the molar absorption coefficient of the acceptor at λ. In the present case, $K^2 = 2/3$, $N = 1.336$ and $\varphi = 0.15$ for HSA. Therefore, according to Eqs. (5), (6), (7) and Fig. S4, $J = 3.6 \times 10^{-14}$ cm^3 L mol^{-1}, $E = 0.36$, $R_0 = 3.17$ nm and $r = 3.6$ nm. The value of r is less than 8 nm and $0.5R_0 < r < 1.5R_0$, suggesting energy transfer from HSA to dinuclear Zn(II) complex occurs with high probability. Furthermore, the value of r is higher than R_0 and it indicates the presence of a static quenching mechanism in the interaction of HSA and complex [74].

Molecular docking of the Zn complex with DNA

The Zn(II) complex was docked to the best conformer of DNA obtained from the MD simulation. The results revealed that the Zn complex fitted into the DNA major groove with the binding energy of −7.7 kcal mol^{-1}, indicating a high binding affinity between DNA and the complex (Fig. 10). This result is in consistent with UV–Vis spectroscopy and fluorescence quenching results. There are four categories of hydrophobic contacts between the complex atoms and bases of DNA, including, DC 9, DG 10, DG 11 and DC 15 (Fig. 11). Furthermore, complex forms a hydrogen bond with DC 14, thus this nucleotide plays a significant role in stabilizing of Zn(II) complex interactions.

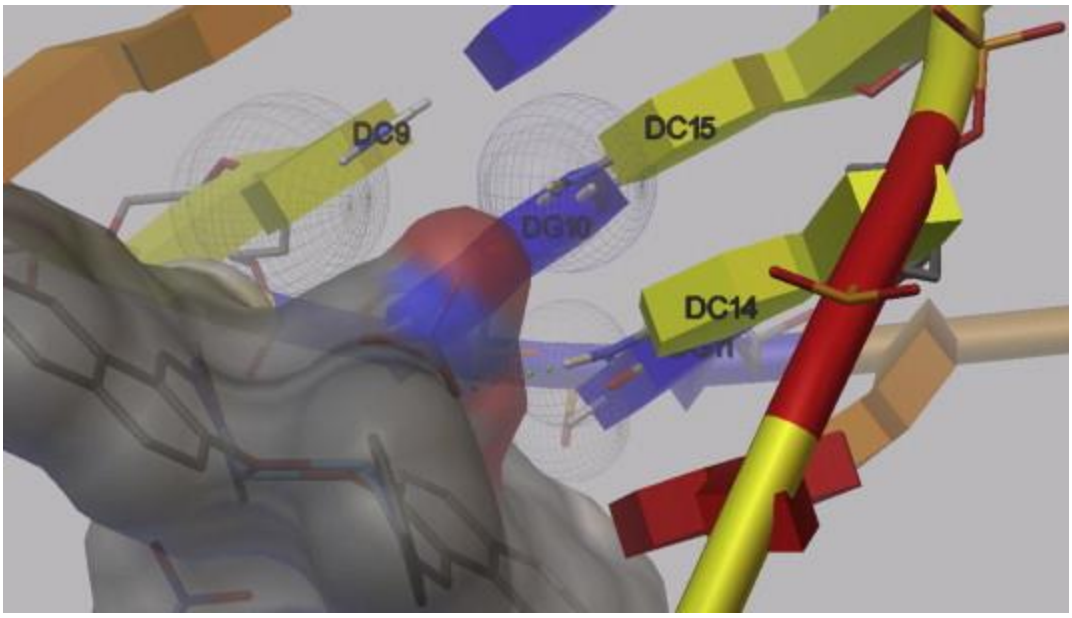

Fig. 10. The docking pose of Zn complex-DNA (the small green spheres show H-bond interaction).

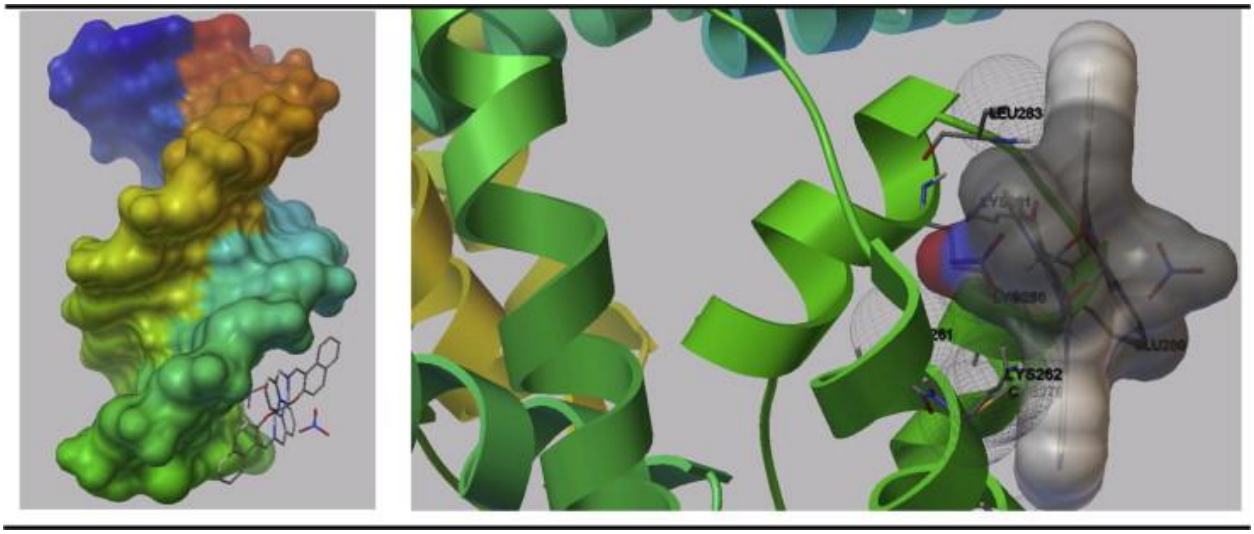

Fig. 11. (Left): Presentation of the interaction of Zn(II) complex with the major groove side of DNA. (Right): The docking pose of Zn(II) complex-HSA (π-cation interaction showed as yellow cone).

Molecular docking of the Zn complex with HSA

HSA is the most abundant protein in human blood plasma and consists of 585 amino acids, with three α-helical domains (I, II and III), each containing two subdomains (A and B) [75]. HSA

transports drugs, hormones, fatty acids, and other compounds, and maintains osmotic pressure, among other functions [76], [77]. The previous crystal structure studies showed that most ligands are binded to one of the two binding sites in subdomains IIA and IIIA [78], [79], [80], [81], [82]. Also, D-shaped cavity in subdomain IB is the binding site of some compounds [83], [84], [85]. The Zn(II) complex was docked to the best conformer of HSA obtained from the MD simulation. The best energy-ranked result of the interaction between complex and protein in all runs of docking procedure is shown in Fig. 11. As seen Zn(II) complex was situated within subdomain IIA in site 1 with the binding energy of −11.14 kcal mol^{-1}. Furthermore, this compound was adjacent to some hydrophobic residues in subdomain IIA of HSA (Ala 210, Ala 213, Val 482 and Leu 481). On the other hand, complex was able to form a π-cation interaction with Lys 286, thus this residue plays a significant role in stabilizing of Zn complex interactions (Fig. S5).

Conclusion

In this study, a dinuclear Zn(II) Schiff base complex, **$Zn_2L_2(NO_3)_2$**, was synthesized from reaction of $Zn(NO_3)_2$ and a tridentate ligand, **HL**, at ambient temperature. The ligand and complex were characterized by FT-IR, ^{1}H NMR, ^{13}C NMR and elemental analysis (CHN). Furthermore, structure of Zn(II) Schiff base complex was determined by single-crystal X-ray analysis. The complex, **$Zn_2L_2(NO_3)_2$**, is centrosymmetric dimer in which deprotonated phenolates bridge the two Zn(II) atoms and link the two halves of the dimer. In structure, the Zinc(II) ions have a highly distorted six-coordinate structure, bonded to two oxygen atoms of a bidentate nitrate group, the nitrogen atom of pyridine, the nitrogen atom of imine group and the two oxygen atoms of two phenolate groups. Moreover, DNA and HSA binding of complex were investigated using fluorescence quenching, UV–Vis spectroscopy, molecular docking and molecular dynamics simulation methods. Fluorescence quenching and UV–Vis spectroscopy results represent that dinuclear Zn(II) complex binds to DNA and HSA with binding constants of $(3.60 \pm 0.18) \times 10^4\ M^{-1}$ and $(1.35 \pm 0.24) \times 10^4\ M^{-1}$, respectively. Molecular docking studies revealed the binding of dinuclear Zn(II) complex to the major groove of DNA and IIA site of HSA by formation of hydrogen bond, π-cation and hydrophobic interactions. These results reflect the strong interaction with DNA and HSA which is in consistent with the fluorescence quenching UV–Vis spectroscopy.

Acknowledgement

The authors are grateful to the Research Council of the University of Isfahan for financial support of this work.

Appendix A. Supplementary material

CCDC 1042425 for Zn2L2(NO3)2 contains the supplementary crystallographic data for this complex. Copies of the data can be obtained, free of charge, on application to CCDC, 12 Union Road, Cambridge CB21EZ, UK (Fax: +44 1223 336033 or e-mail: deposit@ ccdc.cam.ac.uk). Supplementary data associated with this article can be found, in the online version, at http://dx.doi.org/10.1016/ j.molstruc.2015.04.033.

References

[1] S. Tabassum, M. Zaki, M. Ahmad, M. Afzal, S. Srivastav, S. Srikrishna, F. Arjmand, Eur. J. Med. Chem. 83 (2014) 141–154.

[2] K. Dhahagani, S.M. Kumar, G. Chakkaravarthi, K. Anitha, J. Rajesh, A. Ramu, G. Rajagopal, Spectrochim. Acta A 117 (2014) 87–94.

[3] M. Galanski, M.A. Jakupec, B.K. Keppler, Curr. Med. Chem. 12 (2005) 2075–2094.

[4] N. Pravin, N. Raman, Eur. J. Med. Chem. 85 (2014) 675–687.

[5] J.R. Anacona, J.L. Rodriguez, J. Camus, Spectrochim. Acta A129 (2014) 96–102.

[6] M.L. Sundararajana, T. Jeyakumar, J. Anandakumaran, B. Karpanai, Spectrochim. Acta A131 (2014) 82–93.

[7] F. Arjmand, F. Sayeed, M. Muddassi, J. Photochem. Photobiol. B 103 (2011) 166–179.

[8] H.H. Thorp, Chem. Biol. 5 (1998) R125–R127.

[9] G.A. Papoian, W.F. DeGrado, M.L. Klein, J. Am. Chem. Soc. 125 (2003) 560–569.

[10] M. Anjomshoa, S.J. Fatemi, M. Torkzadeh-Mahani, H. Hadadzadeh, Spectrochim. Acta A 127 (2014) 511–520.

[11] A.K. Singh, O.P. Pandey, S.K. Sengupta, Spectrochim. Acta A 113 (2013) 393–

399.
[12] R. Palchaudhuri, P.J. Hergenrother, Curr. Opin. Biotechnol. 18 (2007) 497–503.
[13] M. Çesmea, A. Gölcü, I. Demirtas, Spectrochim. Acta A 135 (2015) 887–906.
[14] F. Arjmand, M. Aziz, Eur. J. Med. Chem. 44 (2009) 834–844.
[15] N. Arshad, N. Abbas, M.H. Bhatti, N. Rashid, M.N. Tahir, S. Saleem, B. Mirza, J. Photochem. Photobiol. B 117 (2012) 228–239.
[16] J.A. Smith, F.R. Keene, F. Li, J.G. Collins, Noncovalent DNA binding of metal complexes, in: J. Reedijk, K. Poeppelmeier (Eds.), Comprehensive Inorganic Chemistry II: from Elements to Applications, Elsevier, Oxford, UK, 2013, pp. 709–750.
[17] N. Shahabadi, S. Kashanian, F. Darabi, Eur. J. Med. Chem. 45 (2010) 4239–4245.
[18] A. Jayamani, N. Sengottuvelan, G. Chakkaravarthi, Polyhedron 81 (2014) 764–776.
[19] A.E. Radi, A.E. El-Naggar, H.M. Nassef, Electrochim. Acta 129 (2014) 259–265.
[20] M.T. Behnamfar, H. Hadadzadeh, J. Simpson, F. Darabi, A. Shahpiri, T. Khayamian, M. Ebrahimi, H. Amiri Rudbari, M. Salimi, Spectrochim. Acta A 134 (2015) 502–516.
[21] C. Ozluer, H.E.S. Kara, J. Photochem. Photobiol. B 138 (2014) 36–42.
[22] A. Barik, B. Mishra, A. Kunwar, K.I. Priyadarsini, Chem. Phys. Lett. 436 (2007) 239–243.
[23] F. Janati Fard, Z. Mashhadi Khoshkhoo, H. Mirtabatabaei, M.R. Housaindokht, R. Jalal, H. Eshtiagh Hosseini, M.R. Bozorgmehr, A.A. Esmaeili, M. Javan Khoshkholgh, Spectrochim. Acta A 97 (2012) 74–82.
[24] Stoe, Cie, Program for the Acquisition and Analysis of Data XeAREA, Version 1.30, Stoe&Cie GmbH, Darmatadt, Germany, 2005.
[25] Stoe & Cie, Program for Data Reduction and Absorption Correction Xe; RED, Version 1.28b, Stoe&Cie GmbH, Darmatadt, Germany, 2005.
[26] Stoe & Cie, Program for Crystal Optimization for Numerical Absorption Correction Xe; SHAPE, Version 2.05, Stoe&Cie GmbH, Darmatadt, Germany, 2004.
[27] M.C. Burla, R. Caliandro, M. Camalli, B. Carrozzini, G.L. Cascarano, L. De Caro, C.

Giacovazzo, G. Polidori, R. Spagna, J. Appl. Crystallogr. 38 (2005) 381–388.
[28] G.M. Sheldrick, SHELXL97, University of Göttingen, Göttingen, Germany, 1997.
[29] A.E. Radi, A. Eissa, H.M. Nassef, J. Electroanal. Chem. 717–718 (2014) 24–28.
[30] M. Tariqa, N. Muhammad, S. Ali, J.H. Shirazi, M.N. Tahir, N. Khalid, Spectrochim. Acta A 122 (2014) 356–364.
[31] C.N. Pace, F. Vajdos, L. Fee, G. Grimsley, T. Gray, Protein. Sci. 4 (1995) 2411–2423.
[32] H.J.C. Berendsen, D. Van der Spoel, R. Van Drunen, Comput. Phys. Commun. 91 (1995) 43–56.
[33] E. Lindah, B. Hess, D. Van der Spoel, J. Mol. Model. 7 (2001) 306–317.
[34] W.F. Van Gunsteren, S.R. Billeter, A.A. Eising, P.H. Hünenberger, P.K.H.C. Krüger, A.E. Mark, W.R.P. Scott, I.G. Tironi, Biomolecular Simulation: The GROMOS96 Manual and User Guide, VdfHochschulverlag AG, Zürich, 1996.
[35] W.F. Van Gunsteren, X. Daura, A.E. Mark, Encyclopedia of Computational Chemistry, Wiley and Sons, P. Von RagueSchleyer, Chichester, UK, 1998.
[36] H.J.C. Berendsen, J.P.M. Postma, W.F. Van Gunstetren, J. Hermans, Intermolecular Forces, B. Pullman, Reidel, Dordrecht, The Netherlands, 1981.
[37] B. Hess, H. Bekker, H.J.C. Berendsen, J. Fraaije, J. Comput. Chem. 18 (1997) 1463–1472.
[38] T. Darden, D. York, L. Pedersen, J. Chem. Phys. 98 (1993) 10089–10092.
[39] U. Essmann, L. Perera, M.L. Berkowitz, T. Darden, H. Lee, L.G. Pedersen, J. Chem. Phys. 103 (1995) 8577–8593.
[40] G.M. Morris, D.S. Goodsell, R.S. Halliday, R. Huey, W.E. Hart, R.K. Belew, A.J. Olson, J. Comput. Chem. 19 (1998) 1639–1662.
[41] M. Khorshidifard, H. Amiri Rudbari, Z. Kazemi-Delikani, V. Mirkhani, R. Azadbakht, J. Mol. Struct. 1081 (2015) 494–505.
[42] S.S. Tandon, S. Chanderb, L.K. Thompson, J.N. Bridson, V. McKeec, Inorg. Chim. Acta 219 (1994) 55–65.
[43] K.M. Sureshan, T. Uchimaru, Y. Yao, Y. Watanabe, CrystEng-Comm 10 (2008) 493–496.
[44] S. Sharma, T.P. Radhakrishnan, J. Phys. Chem. B 107 (2003) 147–156.

[45] A. Kanazawa, T. Ikeda, J. Abe, J. Am. Chem. Soc. 123 (2001) 1748–1754.
[46] C.Q. Wan, X.D. Chen, T.C.W. Mak, CrystEngComm 10 (2008) 475–478.
[47] X.P. Zhou, X. Zhang, S.H. Lin, D. Li, Cryst. Growth Des. 7 (2007) 485–487.
[48] D. QuiEonero, C. Garau, C. Rotger, A. Frontera, P. Ballester, A. Costa, P.M. Dey, Angew. Chem. Int. Ed. 41 (2002) 3389–3392.
[49] P.D. Hoog, P. Gamez, I. Mutikainen, U. Turpeinen, J. Reedijk, Angew. Chem. Int. Ed. 43 (2004) 5815–5817.
[50] F.H. Haghighi, H. Hadadzadeh, F. Darabi, H. Farrokhpour, M. Daryanavard, H. Amiri, J. Mol. Struct. 1040 (2013) 98–111.
[51] M. Sirajuddin, S. Ali, A. Badshah, J. Photochem. Photobiol. B 124 (2013) 1–19.
[52] K. Abdi, H. Hadadzadeh, M. Weil, H. Amiri, Inorg. Chim. Acta 416 (2014) 109–121.
[53] A. Jayamani, V. Thamilarasan, N. Sengottuvelan, P. Manisankar, S.K. Kang, Y. Kim, V. Ganesan, Spectrochim. Acta A 122 (2014) 365–374.
[54] R. Gup, C. Gökçe, S. Aktürk, Spectrochim. Acta A 134 (2015). 484-49.
[55] J.K. Barton, A.T. Danishefsky, J.M. Goldberg, J. Am. Chem. Soc. 106 (1984) 2172–2176.
[56] C. Metcalfe, C. Rajput, J.A. Thomas, J. Inorg. Biochem. 100 (2006) 1314–1319.
[57] S. Tabassum, G. Chandra Sharma, A. Asim, A. Azam, R.A. Khan, J. Organomet. Chem. 713 (2012) 123–133.
[58] M.N. Patel, M.R. Chhasatia, P.A. Dosi, H.S. Bariya, V.R. Thakkar, Polyhedron 29 (2010) 1918–1924.
[59] K. Dhara, J. Ratha, M. Manassero, X. Wang, S. Gao, P. Banerjee, J. Inorg. Biochem. 101 (2007) 95–103.
[60] F. Arjmand, A. Jamsheera, D.K. Mohapatra, J. Photochem. Photobiol. B 121 (2013) 75–85.
[61] X.B. Fu, G.T. Weng, D.D. Liu, X.Y. Le, J. Photochem. Photobiol. A 276 (2014) 83–95.
[62] M.J. Waring, J. Mol. Biol. 13 (1965) 269–282.
[63] P. Fromherz, B. Rieger, J. Am. Chem. Soc. 108 (1986) 5361–5362.
[64] K. Ghosh, N. Tyagi, P. Kumar, U.P. Singh, Inorg. Chim. Acta 412 (2014) 20–26.

[65] F. Darabi, H. Hadadzadeh, M. Ebrahimi, T. Khayamian, H. Amiri, Inorg. Chim. Acta 409 (2014) 379–389.
[66] J.R. Lakowicz, Springer Science, New York, 2006.
[67] D.D. Li, J.L. Tian, W. Gu, X. Liu, S.P. Yan, Eur. J. Inorg. Chem. (2009) 5036–5045.
[68] K. Abdi, H. Hadadzadeh, M. Salimi, J. Simpson, A. DehnoKhalaji, Polyhedron 44 (2012) 101–112.
[69] N. Shahabadi, A. Khorshidi, M. Mohammadpour, Spectrochim. Acta A 122 (2014) 48–54.
[70] H. Farrokhpour, H. Hadadzadeh, F. Darabi, F. Abyar, H. Amiri Rudbari, T. Ahmadi-Bagheri, RSC Adv. 4 (2014) 35390–35404.
[71] P. Banerjee, S. Ghosh, A. Sarkar, S.C. Bhattacharya, J. Lumin. 131 (2011) 316–321.
[72] A.K. Shaw, S.K. Pal, Photochem. Photobiol. B90 (2008) 187–197.
[73] N. Fani, A.K. Bordbar, Y. Ghayeb, Spectrochim. Acta A 103 (2013) 11–17.
[74] Z. Jannesari, H. Hadadzadeh, T. Khayamian, B. Maleki, H. Amiri, Eur. J. Med. Chem. 69 (2013) 577–590.
[75] D.C. Carter, J.X. Ho, Adv. Protein. Chem. 45 (1994) 153–203.
[76] Nature 358 (1992) 209–215.
[77] U. Kragh-Hansen, V.T. Chuang, M. Otagiri, Biol. Pharm. Bull. 25 (2002) 695–704.
[78] G. Sudlow, D.J. Birkett, D.N. Wade, Mol. Pharmacol. 11 (1975) 824–832.
[79] G. Sudlow et al., Mol. Pharmacol. 12 (1976) 1052–1061.
[80] J. Ghuman et al., J. Mol. Biol. 353 (2005) 38–52.
[81] I. Petitpas et al., J. Biol. Chem. 276 (2001) 22804–22809.
[82] J. Ryan et al., J. Struct. Biol. 174 (2011) 84–91.
[83] P.A. Zunszain et al., BMC Struct. Biol. 3 (2003) 6.
[84] P.A. Zunszain et al., J. Mol. Biol. 381 (2008) 394–406.
[85] D. Buttar et al., Bioorg. Med. Chem. 18 (2010) 7486–7496